Cancer Letters 396 (2017) 117–129

Contents lists available at ScienceDirect

Cancer Letters

journal homepage: www.elsevier.com/locate/canlet

Original Article

Metabolic re-wiring of isogenic breast epithelial cell lines following epithelial to mesenchymal transition

Skarphedinn Halldorsson [a, b, *, 1], Neha Rohatgi [a, b, 1], Manuela Magnusdottir [a], Kumari Sonal Choudhary [a, b], Thorarinn Gudjonsson [b, c], Erik Knutsen [e], Anna Barkovskaya [f, g], Bylgja Hilmarsdottir [f], Maria Perander [e], Gunhild M. Mælandsmo [f, h], Steinn Gudmundsson [a, d], Óttar Rolfsson [a, b]

[a] Center for Systems Biology, University of Iceland, Reykjavik, Iceland
[b] Biomedical Center, University of Iceland, Reykjavík, Iceland
[c] Department of Anatomy, Faculty of Medicine, and Department of Laboratory Hematology, University Hospital, Reykjavik, Iceland
[d] School of Engineering and Natural Sciences, University of Iceland, Reykjavik, Iceland
[e] Department of Medical Biology, UiT – The Arctic University of Norway, Tromsø, Norway
[f] Department of Tumor Biology, Institute for Cancer Research, Norwegian Radium Hospital, Oslo, Norway
[g] Department of Circulation and Medical Imaging, Faculty of Medicine, Norwegian University of Science and Technology, Trondheim, Norway
[h] Department of Pharmacy, UiT – The Arctic University of Norway, Tromsø, Norway

ARTICLE INFO

Article history:
Received 10 November 2016
Received in revised form
3 March 2017
Accepted 12 March 2017

Keywords:
EMT
Metabolism
Genome scale models
Breast cancer

ABSTRACT

Epithelial to mesenchymal transition (EMT) has implications in tumor progression and metastasis. Metabolic alterations have been described in cancer development but studies focused on the metabolic re-wiring that takes place during EMT are still limited. We performed metabolomics profiling of a breast epithelial cell line and its EMT derived mesenchymal phenotype to create genome-scale metabolic models descriptive of both cell lines. Glycolysis and OXPHOS were higher in the epithelial phenotype while amino acid anaplerosis and fatty acid oxidation fueled the mesenchymal phenotype. Through comparative bioinformatics analysis, PPAR-γ1, PPAR- γ2 and AP-1 were found to be the most influential transcription factors associated with metabolic re-wiring. *In silico* gene essentiality analysis predicts that the LAT1 neutral amino acid transporter is essential for mesenchymal cell survival. Our results define metabolic traits that distinguish an EMT derived mesenchymal cell line from its epithelial progenitor and may have implications in cancer progression and metastasis. Furthermore, the tools presented here can aid in identifying critical metabolic nodes that may serve as therapeutic targets aiming to prevent EMT and inhibit metastatic dissemination.

Introduction

Epithelial to mesenchymal transition (EMT) is a process where cells of epithelial origin lose their polarity and cell–cell adhesion and change their phenotype to mesenchymal-like cells. EMT is a fundamental process in embryonic development allowing cells to detach from the newly formed epithelium and migrate to other parts of the developing embryo [1,2]. Once they have reached their destination, these epithelial-derived mesenchymal cells revert to their original phenotype via mesenchymal to epithelial transition (MET) and take part in establishing new tissues and organs.

Many carcinomas are known to revive these mechanisms during cancer invasion and metastasis. EMT shifts the phenotype of the polarized epithelial cell, bound to its neighbors and extracellular matrix via tight junctions, desmosomes and E-cadherin, to an invasive mesenchymal phenotype that exists largely without direct cell–cell contacts or defined cell polarity. The ability to separate from neighboring cells and penetrate into the surrounding tissues

Abbreviations: EMT, Epithelial to mesenchymal transition; MET, Mesenchymal to epithelial transition; RNA-seq, RNA sequencing; UPLC-MS, Ultra-performance liquid chromatography mass-spectrometry; GEM, Genome scale metabolic model; FBA, Flux balance analysis; GPR, Gene-Protein-Reaction association; TF, Transcription factor.

* Corresponding author. Center for Systems Biology, University of Iceland, Reykjavik, Iceland.
E-mail address: skarph@hi.is (S. Halldorsson).
[1] Equal contribution.

http://dx.doi.org/10.1016/j.canlet.2017.03.019

is believed to be an important initiating step in tumor metastasis [3]. EMT also acts in tumor progression by providing increased resistance to apoptotic agents [4], and by producing supporting tissues that enhance the malignancy of the central tumor [5]. As such, EMT confers on epithelial cells precisely the set of traits that would empower them to disseminate from primary tumors and seed metastases [6].

Metabolic alterations have been shown to play a role in determining cellular phenotypes. For example, knock-down of fructose-1,6-bisphosphatase has been shown to induce EMT in basal-like breast cancer cells [7], while knockdown of ATP citrate lyase has been shown to revert the EMT phenotype in non-small cell lung carcinoma cells [8]. Mutations or epigenetic changes that cause accumulation of certain metabolites have also been shown to induce EMT [9]. While these findings show that metabolic alterations are important for induction and maintenance of a mesenchymal phenotype; studies of the global metabolic changes that occur during EMT are still limited.

Genome scale metabolic models (GEMs) provide descriptions of metabolic phenotypes that can be queried computationally through constraint-based modeling [10]. The building of GEMs and their application to the analysis of metabolism of diverse biological processes is well established [11]. EMT metabolism has so far mainly been investigated through more targeted cell- and molecular biology based approaches. Previous efforts show that systems based analysis, in particular constraint based modeling methods, may provide important insights into EMT metabolism [9,12,13].

Here, we describe the metabolic phenotype of the immortalized, breast epithelial cell line, D492. We compare the metabolic phenotype of D492 to that of its mesenchymal "daughter" cell line, D492M. D492M cells were isolated after a spontaneous EMT event in D492 cells in 3D co-culture with endothelial cells [14]. Although neither of these cell lines are tumorigenic in an *in vivo* setting, they provide an interesting model system to investigate EMT without the need for external stimulation or genetic manipulation. Ultra performance liquid chromatography Mass Spectrometry (UPLC-MS) on spent media was used to quantify uptake and secretion of 43 selected metabolites. These data, coupled with microarray and RNA sequencing expression profiles, were used to build GEMs descriptive of metabolism in the two cell lines. We validated the computationally proposed metabolic phenotypes through enzymatic assays of intracellular ATP, NADH, and glutathione levels together with mitochondrial functionality assays. The GEMs were then used to predict enzymatic reactions and pathways of importance for the metabolic re-programming that occurs during EMT. Some of these reactions, in particular the large neutral amino acid transporter LAT1, appear important for cancer remission following breast cancer treatment. The results represent the construction of the first curated GEMs descriptive of metabolism pre- and post EMT. As such they serve as tools for future investigation of EMT metabolism. Furthermore, the results highlight how GEMs can be applied to the integrated analysis of polyomics data and propose metabolic biomarkers of importance for EMT and metastasis.

Materials and methods

Cell culture

D492 and D492M cells were cultured on collagen coated surfaces or in reconstituted basement membrane (Matrigel, Corning) in H14 serum-free medium as previously described [14] at 37 °C, 5% CO_2. H14 is a fully defined medium consisting of a DMEM/F12 base with 250 ng/ml insulin, 10 mg/ml transferrin, 2.6 ng/ml sodium selenite, 10^{-10} M estradiol, 1.4×10^{-6} M hydrocortisone, 5 mg/ml prolactin and 10 ng/ml EGF. Proliferation and ATP concentration was measured with a CellTiter Glo™ assay (Promega). Cell volume was calculated based on diameter measurements obtained from a Countess cell counting instrument (Invitrogen). For UPLC-MS, cells were seeded in triplicates into 24-well plates in 400 μL H14 medium at 15,000 cells/cm^2. Media was collected from cultures after 24 and 48 h along with cell-free controls, centrifuged to remove cellular debris and stored at −80 °C until further analysis.

Cell profiling

Total RNA sequence profiles were obtained for D492 and D492M as outlined in supplementary methods (**Additional file 2**). Microarray expression profiles of D492 and D492M cells were obtained from [14]. Medium metabolites were measured using an established metabolomics pipeline. Both the metabolite isolation procedure and metabolomic pipeline analysis were adapted from Paglia et al., 2014 [15]. The methods are explained in SI Materials and Methods. To account for differences in cell weight and growth rate, the measured metabolite concentrations were normalized to cell weight and growth rates as previously described [16]. Seahorse XFe-96 metabolic extracellular flux analyzer (Seahorse Biosciences) was used to measure the oxygen consumption rate (OCR) and the extracellular acidification rate (ECAR). See SI Materials and methods for details. Intracellular NAD^+/NADH and GSH/GSSG were assayed with respective Glo™ kits from Promega. Additional glucose and lactate measurements were performed in an ABL 90 blood gas analyzer (Radiometer, Brønshøj, Denmark).

Generation of a breast tissue specific metabolic model

RNA-seq data from the D492 and D492M cells were used to create a breast tissue specific model from the human metabolic reconstruction RECON2 [17] as follows. All genes with expression values exceeding a fixed cut-off value in either the D492 or D492M data sets that were also present in RECON2 were identified. The gene-protein-reaction rules (GPRs) of RECON2 were then used to identify the associated metabolic reactions and the FASTCORE model building algorithm [18] used to build a functional metabolic network from the list of reactions. The resulting network, referred to as the EMT model, was manually curated in order to ensure that no major pathways and metabolites were missing. Details of the model construction are provided in SI Materials and methods.

Construction and analysis of the D492 and D492M GEMs

The EMT model was used to create models of the epithelial D492 cells and mesenchymal D492M cells. Random sampling was first used to estimate flux ranges of all the reactions in the EMT model. While the RNA-seq data had considerably more coverage, it lacked the necessary replicates. Therefore, the microarray expression data was used to constrain the EMT model to simulate the effects of up and downregulated genes on reaction flux. This gave rise to models EPI (epithelial) and MES (mesenchymal) once metabolomics constraints had been applied. The two models generated in this manner therefore had the same stoichiometry but different constraints on reaction fluxes as defined by differential expression of metabolic genes and extracellular metabolomics measurements. Deriving the two models from a common model was done because the D492M cells initially arose from D492 cells and this facilitated both model curation and subsequent model comparisons. See SI Material and methods for details.

Analysis of the EPI and MES models

We used flux balance analysis (FBA) [19,20] and the generic biomass reaction present in RECON2 to predict the maximum growth rates of the EPI and MES models. Random sampling [21] was used to compare the two. An optimization algorithm was used to identify targets for transforming the epithelial phenotype into the mesenchymal phenotype and vice-versa. The algorithm works by relaxing flux bounds for reactions in one model in order to obtain a flux distribution that is as close as possible to the flux distribution in the other [13]. The genes corresponding to these reactions were identified via the GPRs and the associated transcription factors then located in SABiosciences' proprietary database (http://www.sabiosciences.com/chipqpcrsearch). Gene essentiality analysis was performed on the EPI and MES models by simulating single gene knockouts with FBA.

Results

D492M cells show reduced size and growth rate compared to D492 cells

In order to accurately calculate metabolic uptake and secretion rates morphological parameters including cell size and weight, and proliferation rates were established. In 2D culture, D492 cells display the typical cobblestone morphology of epithelial cells while D492M cells have acquired the spindle-like phenotype of mesenchymal cells, characterized by multiple membrane protrusions (Fig. 1A**, top row**). In 3D culture, D492 cells form organized, branching structures while D492M form colonies that have lost polarity and cell–cell contact (Fig. 1A**, bottom row**). Growth rate measurements in 2D indicated population doubling times of 25 h for D492 cells and

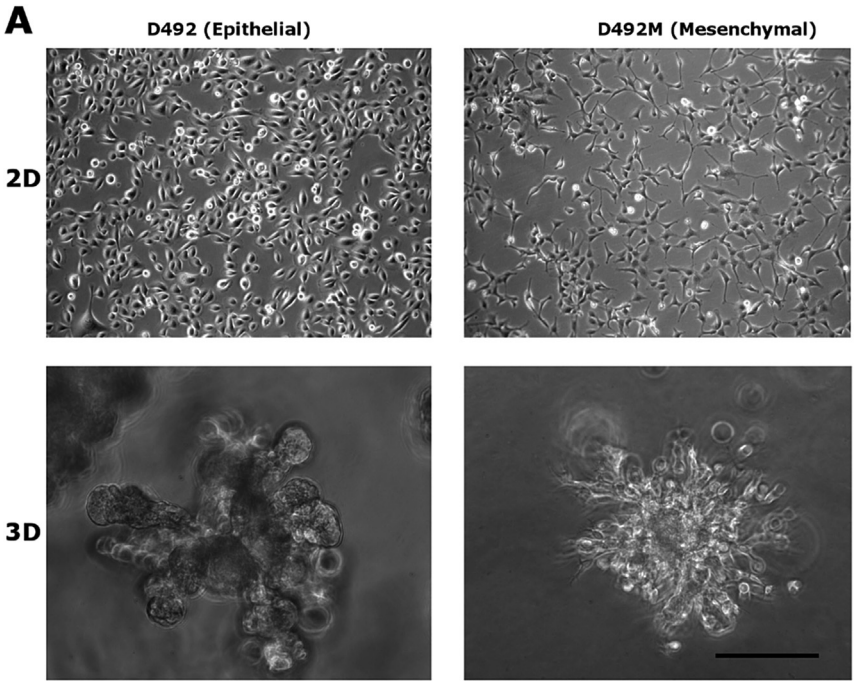

B

	D492 (Epithelial)	**D492M** (Mesenchymal)
Proliferation rate (h^{-1})	0,028	0,022
Dry weight (*ng/cell*)	1	0,53
Volume (*pL/cell*)	1,7	1,4

Fig. 1. Phenotypic characteristics of D492 and D492M cells (A) D492 cells (top left) have the typical almond morphology of epithelial cells when grown on culture plastic. When cultured in rBM/matrigel, D492 form branching lobular-like structures reminiscent of terminal duct lobular unit *in vivo* (bottom left). In contrast, D492M cells form clusters of disorganized mesenchymal like cells (bottom right). When isolated and re-grown on tissue culture plastic, these cells retain a mesenchymal phenotype (top right). Bar = 100 μm. (B) Measured growth rates, dry weight and volume of D492 and D492M cells.

roughly 32 h for D492M cells, corresponding to growth rates of 0.028 h^{-1} and 0.022 h^{-1}. We subsequently calculated the volume and measured the dry-weight of D492 and D492M cells. D492 cells are larger than D492M cells with an average volume of 1700 fL compared to 1400 fL of D492M cells. Dry weights were measured at 1 ng and 0.53 ng, respectively (Fig. 1B). In summary, D492 and D492M are isogenic cell lines with epithelial and mesenchymal phenotypes, respectively. D492M show reduced size, mass and proliferation rate compared to the parental D492 cell line.

Extracellular metabolomics changes are indicative of differences in metabolism in D492 following EMT

In order to distinguish between the metabolic phenotypes associated with D492 and D492M we carried out metabolic analysis of spent media after 48 h of cell culture. Targeted metabolomic analysis of a total of 43 metabolites in the growth medium afforded quantitative consumption rates of 7 compounds in central carbon metabolism, 23 amino acids or derivatives thereof, 6 nucleotide derivatives, 5 vitamins and 2 choline derivatives. Metabolite uptake of D492 epithelial cells was generally higher than that of D492M mesenchymal cells, consistent with their increased proliferation rate (SI Fig. 1).

During growth the two cell lines consumed and secreted metabolites reflecting their nutritional requirements and active metabolic pathways. D492 cells had higher glucose consumption and lactate secretion rates, as compared to D492M cells. The calculated glucose to lactate ratio of D492 cells was 1.48 mol of lactate per mole glucose but only 0.8 mol of lactate per mole glucose in D492M cells, suggestive of altered utilization of carbons originating from glucose.

Apart from glucose and lactate, the most prominent differences were observed in the amino acids glutamine, threonine, lysine, arginine, cystine, and (iso)-leucine (Fig. 2). While the altered profiles of these amino acids may reflect demand due to protein synthesis, catabolism of amino acids also serves to fuel flux through the TCA cycle. We therefore hypothesized that anaplerosis of amino acids may contribute differently to TCA cycle flux between the two cell lines. To explore this further, we turned to genome scale metabolic modeling.

D492 and D492M metabolism captured in GEMs

In order to obtain a holistic description of D492 and D492M metabolism, we built GEMs of both phenotypes based on the generic human metabolic reconstruction RECON2 [17] using the measured metabolite uptake and secretion rates and transcriptomic data (Fig. 3A). The number of overlapping genes between the RNA-seq data set and RECON2 was 1284 but 338 additional genes were needed in order to make a functional model representing both cell lines, referred to as the EMT metabolic model (Fig. 3B). Cell specific models were obtained by mapping microarray expression data to the EMT model. Based on the selected cut-off value, a total of 74 genes were under-represented in the D492M expression data and 65 in the D492 expression data.

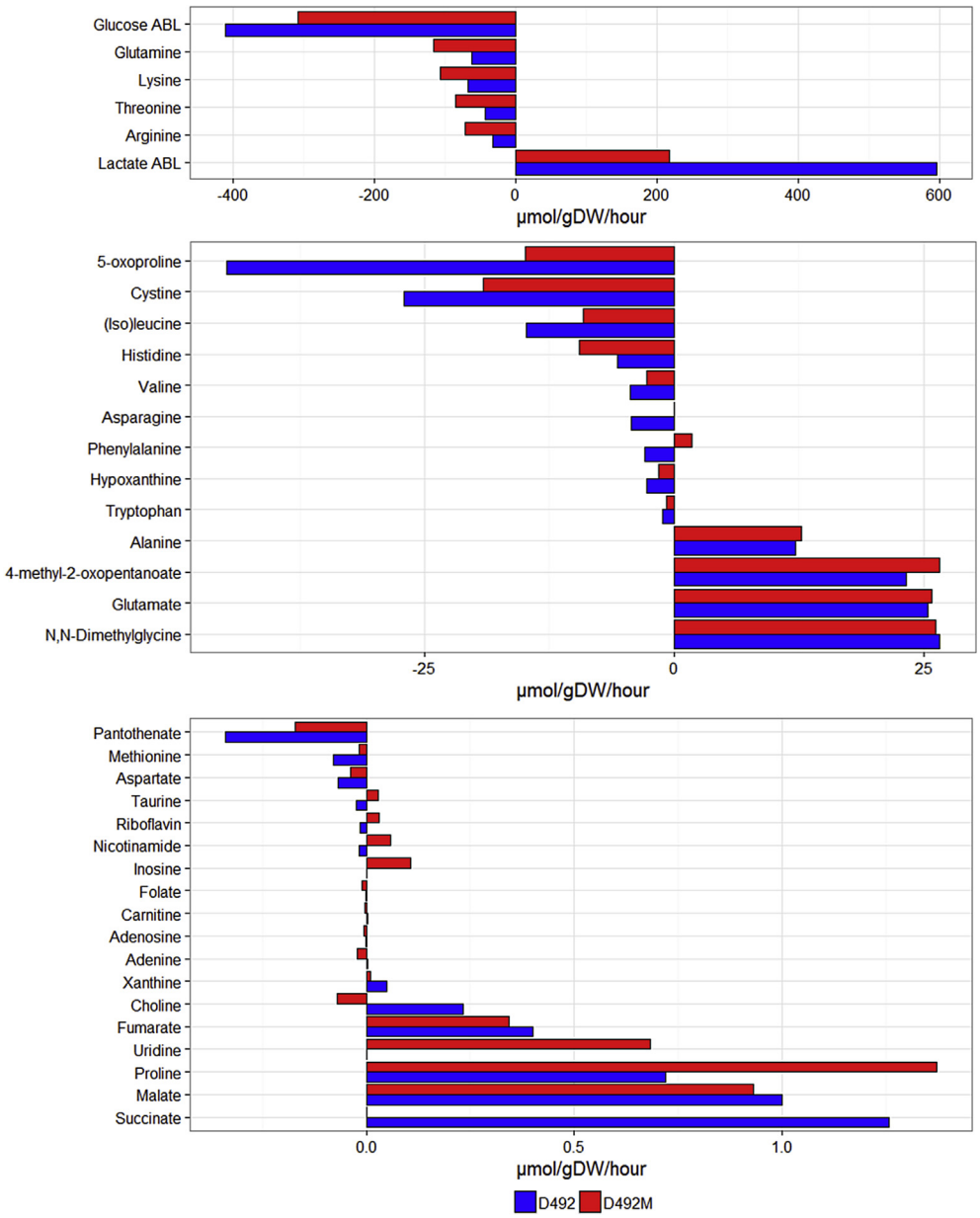

Fig. 2. Metabolite uptake and secretion rates in D492 and D492M cells. Mean metabolite uptake and secretion rates presented *as µmol* per *grams dry-weight* per *hour* were calculated as described in [16] based on the UPLC-MS results, ABL90 measurements, growth rates and dry-weight calculations. Uptake rates are represented as negative values, secretion as positive values. D492 cells represented with blue bars, D492M cells represented with red bars. Bars represent mean values of 3 biological replicates of each phenotype and 3 control samples. (For interpretation of the references to color in this figure legend, the reader is referred to the web version of this article.)

After restricting the corresponding fluxes and applying constraints based on measured cell specific uptake and secretion rates, we obtained the functional EPI and MES models. Comparison between RECON2 and the EMT model is provided in Fig. 3C.

Altered mitochondrial activity and validation of predicted differences in energy metabolism

In order to validate whether the computational models were descriptive of D492 and D492M cell growth, we compared the predicted maximum growth rates of the EPI and MES models obtained with FBA to the measured growth rates of the cells (Fig. 1b). The ratio between the growth rates of the EPI and MES models is 1.4, which is in agreement with the measured growth rates ratio of 1.3 between D492 and D492M cells. The predicted growth rates were not expected to match the experimental values quantitatively since the biomass function is not necessarily representative of breast epithelial cells [22] and maximizing biomass may not be the "true" cellular objective of the D492 and D492M cells.

The difference in predicted growth rates between the EPI and MES models was traced to decreased activity of cardiolipin synthase in MES model. A demand for mitochondrial ATP was added to the EPI and MES models and FBA was used to estimate the maximum ATP generation. According to these estimates, maximal mitochondrial ATP production is 4.4 times higher in the EPI model than in the MES model. Mitochondrial staining of D492 and D492M did not reveal apparent differences in overall mitochondrial abundance (Fig. 4a). This was further confirmed with flow cytometry (data not shown). The D492 cells show a strong perinuclear mitochondrial staining while D492M cells show mitochondria

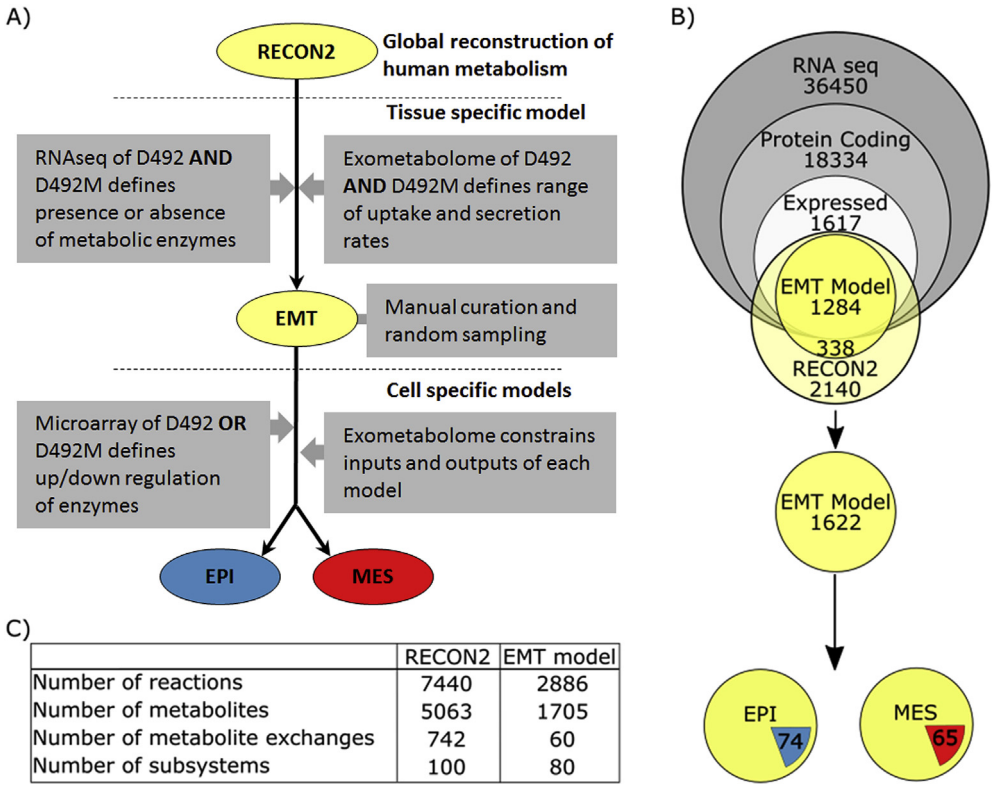

Fig. 3. EMT Model reconstruction: (A) An overview of the model reconstruction. Gene expression data and mass spectrometry data for epithelial (D492) and mesenchymal (D492M) cells was combined with the human metabolic reconstruction (RECON2) to make a metabolic model of EMT. The EMT model was further constrained with differential expression from microarray data and mass spectrometry data to afford two genome scale models descriptive of metabolism in D492 and D492M. (B) Details of the model reconstruction. RECON2 was combined with an RNA-seq dataset containing 36,450 unique transcripts, of which 18,334 were protein coding. Transcripts with expression values above a given cut-off value in either cell were included, leaving 1617 genes of which 1284 were present in RECON2. Microarray expression data was then used to define differentially expressed genes between D492 and D492M cells. The fluxes in the EMT model were then constrained using this information together with cell specific metabolomics data to generate phenotype specific models referred to as the EPI and MES models. The arcs in blue and red represent the number of genes over-represented in the microarray dataset for D492 and D492M respectively. (C) Overlap of reactions, metabolites and subsystems between the generic RECON2 model and the EMT model. (For interpretation of the references to color in this figure legend, the reader is referred to the web version of this article.)

placement within the cytosol indicative of mesenchymal front-rear polarity. These data suggest altered mitochondrial function in D492 vs. D492M as opposed to a quantitative effect. Differences in energy metabolism were further confirmed through measurements of the glycolytic vs. oxidative phosphorylation contribution to ATP generation. Both glycolytic and oxidative phosphorylation activity was increased in D492 cells as compared to D492M cells (Fig. 4b). Furthermore, these data showed that D492 cells have higher spare capacity to perform oxidative phosphorylation as compared to the D492M cells (Fig. 4c) and corroborate the metabolic phenotypes captured by the EPI and MES models.

These measurements along with the metabolic phenotypes predicted by the EPI and MES models suggest altered energy metabolism in the two cell lines. In order to validate the proposed metabolic phenotypes, we measured selected energy metabolites using enzyme assays (Table 1). ATP concentration in D492 was significantly higher than in D492M. Total NAD(H) concentration and the ratio of NAD^+/NADH were also higher in D492 as compared to D492M (5.66 vs. 4.52). Glutathione was found to be primarily in the non-oxidized form in both cell lines although the total concentration was considerably higher in D492.

TCA cycle flux and oxidative phosphorylation is altered following EMT in D492

Random sampling was used to estimate flux distributions in the EPI and MES models. Comparisons of flux distributions using two-sample Kolmogorov–Smirnov test identified the metabolic reactions and pathways with altered activity between the two models. The predicted global metabolic alterations that occur in D492 following EMT are shown in SI Fig. 5. Reactions involved in the N- and O-glycan metabolism as well as keratin sulfate metabolism carry far higher flux in the MES model than the EPI model. In contrast, all the reactions involved in purine synthesis and cysteine metabolism carry higher flux in the EPI model than in the MES model.

Fig. 5 shows specific differences in calculated flux distributions through reactions in central carbon metabolism in the EPI and MES models and illustrates predicted differences between D492 and D492M. In the MES model, glycolytic flux is reversed through phosphoglucomutase resulting in more 3-phosphoglycerate diversion to one carbon metabolism, which is one of the contributors to the production of cytosolic NADPH. Triose phosphate isomerase flux was also reversed in the MES model indicative of a demand for the lipid precursor glycerol phosphate through dihydroxyacetone phosphate.

In the TCA cycle, citrate synthase activity was increased in the MES model. This was due to increased oxidation of (iso)-leucine forming acetyl-CoA equivalents to a greater degree in the MES model. Glutamine was metabolized differently in the EPI and MES models. In the EPI model, glutamine was utilized for purine biosynthesis, while in MES model it contributed to alpha-ketoglutarate in the TCA cycle. Increased activity of argininosuccinate lyase in the MES model provided anaplerotic carbons via

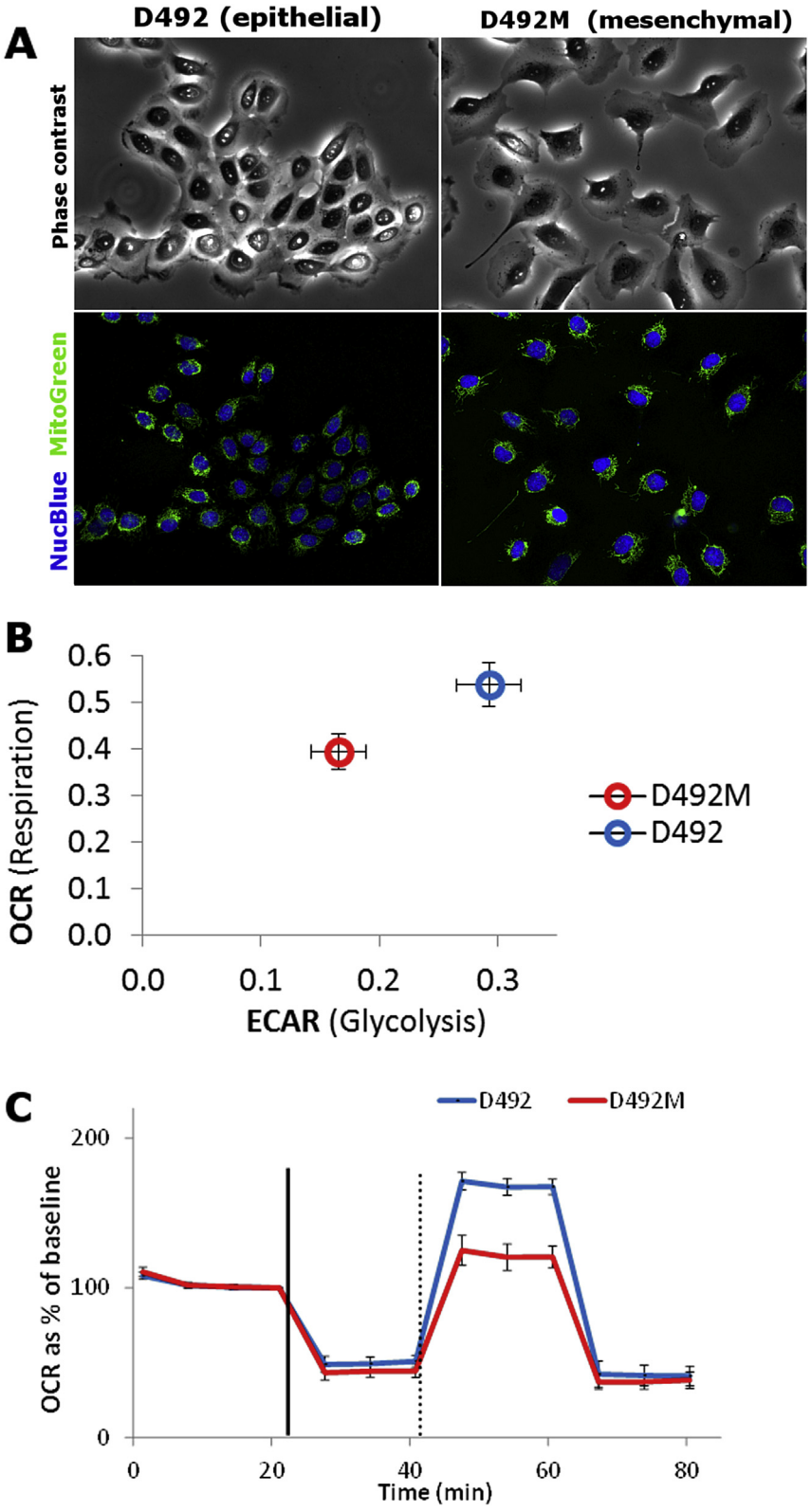

Fig. 4. Respiratory rate and overall respiratory capacity is higher in D492 epithelial cells (A) Mitochondrial staining of D492 (epithelial) cells and D492M (mesenchymal) cells. Although distribution and staining intensity of individual mitochondria appear different in the two cell lines, flow cytometry of stained cells did not indicate significant differences in total mitochondrial staining. (B) Oxygen consumption rate (OCR) and extracellular acidification rate (ECAR) of D492 (blue circle) and D492M cells (red circle) as measured in a Seahorse XF analyzer. OCR is presented as pmol/min and normalized for cell density. ECAR measures the medium acidification (in mpH/hour) do to lactate secretion and is as such a proxy for glycolysis. Data represent 15 technical replicates in 4 separate experiments, error bars represent standard deviation, n = 4. (C) Maximum respiratory capacity in D492 and D492M cells. OCR of D492 (blue line) and D492M (red line) presented over 80 min as percentage of baseline. The solid vertical line marks the time of oligomycin injection, a potent inhibitor of ATP-synthase, and the subsequent drop in oxygen consumption indicates that a similar percentage of ATP is generated via OXPHOS in both cell lines. The dotted vertical line marks the time of FCCP injection, an ETC un-coupler, and the subsequent rise in oxygen consumption indicates that D492 cells have far greater spare respiratory capacity than D492M cells. Data represent one of four separate experiments giving comparable results. Error bars represent standard deviation of 15 technical replicates. (For interpretation of the references to color in this figure legend, the reader is referred to the web version of this article.)

Table 1
Energy metabolite (ATP and NAD(H)) and glutathione (reduced (GSH) and oxidized (GSSG)) concentrations in D492 epithelial and D492M mesenchymal cells. Values represented as *fmol* per *cell* and intracellular concentration in mM ± standard deviation (n = 3).

	D492 Epithelial		D492M Mesenchymal	
	fmol per *cell*	concentration (mM)	*fmol* per *cell*	concentration (mM)
ATP	12.4 ± 0.95	7.29 ± 0.56	7.54 ± 0.44	5.39 ± 0.31
NAD^+	0.85 ± 0.16	0.503 ± 0.096	0.303 ± 0.020	0.216 ± 0.014
NADH	0.15 ± 0.01	0.089 ± 0.004	0.067 ± 0.009	0.048 ± 0.006
GSH	25.42 ± 0.41	14.952 ± 0.239	15.15 ± 0.54	10.82 ± 0.39
GSSG	1.26 ± 0.32	0.740 ± 0.190	0.70 ± 0.38	0.50 ± 0.27

fumarate. Combined, the predicted glycolytic and TCA cycle metabolic phenotypes provide a description of TCA cycle flux rewiring that occurs following EMT in D492 cells.

Identification of metabolic and regulatory genes required for EMT and MET in D492

Having validated the proposed metabolic phenotypes in the EPI and MES models we next identified specific reactions responsible for the metabolic differences observed in the two models. To do this, we calculated which reaction constraints needed to be regulated in the EPI model in order to transform the epithelial phenotype to the mesenchymal phenotype and vice versa for MET. Fig. 6 shows the metabolic subsystems that required regulation, the number of reactions within these subsystems and the number of corresponding genes. The reactions along with their gene identifiers are reported in **Additional file 1.** A total of 88 target reactions required modification for EMT while this number was 335 to revert the mesenchymal phenotype to epithelial. For EMT (Fig. 6A), the highest number of reactions requiring regulation were involved in N-glycan degradation, more specifically keratan sulfate degradation. Most genes requiring regulation were however associated with complex III of the electron transport chain. Other subsystems involved included valine, leucine and isoleucine metabolism and fatty acid oxidation. Out of the 335 target reactions predicted by the models to revert mesenchymal phenotype to epithelial, 288 represented extracellular transport reactions associated with only 5 genes (Fig. 6B). Other important subsystems with altered activity following MET included nucleotide interconversion, glycine, serine, alanine and threonine metabolism and arginine and proline metabolism.

Regulation of transcription is of importance in EMT. We identified transcription factors (TFs) that have been associated with the genes required for EMT and MET in the D492 models using SABiosciences' proprietary database (http://www.sabiosciences.com/chipqpcrsearch). The TFs associated with the genes for EMT and MET overlapped with small differences (**Additional File 1**). PPAR-gamma1, PPAR-gamma2 and AP-1 were associated with the highest number of genes required for both EMT and MET. Sp1 and TFIID exhibited binding to genes associated with EMT only while C/EBPbeta, Msx-1, N-Myc and HFH-1 were predicted to bind to genes only associated with MET. While many of these transcription factors have been shown previously to be of importance in the context of EMT [23,24] the results represent hypothesis of transcription factors important for developmental regulation in the D492 cell model.

Identification of essential genes in the EPI and MES models

Using gene essentiality analysis, we next identified specific metabolic genes in the EPI and MES models that, when knocked out, are likely to be lethal in one cell but not the other (Table 2). Gene targets that are lethal for the EPI model are genes required for reactions of the TCA cycle (fumarase) and oxidative phosphorylation (succinate dehydrogenase (complex II) and ATP synthase) while the genes identified as lethal in the MES model fuel anaplerotic reactions for the TCA cycle. This included a sub-unit of the large neutral amino acid transporter LAT1 and reactions involved acetyl-CoA and fumarate production. These results predict that D492M cells can bypass the electron transport chain by supplying mitochondria with TCA cycle intermediates derived from branched chain or other non-polar amino acids.

Based on the findings above, we argued that high expression of genes predicted to be essential for a mesenchymal phenotype to survive would contribute to cancer relapse or metastasis formation. To investigate whether our predicted lethal genes had relevance to cancer progression, we compared target gene expression in tumors and risk of relapse or distant metastasis over a period of 10 years in a cohort of 3557 breast cancer patients using the Kaplan–Meier Plotter web-tool [25]. In particular, risk of relapse and distant metastasis formation were found to be consistently higher in patients with high expression of the SLC7A5 sub-unit of the LAT1 transporter (Fig. 7).

Discussion

Here we set out to identify modulators of EMT through metabolic systems analysis of the isogenic breast epithelial cell line D492 and its EMT-derivative daughter cell line D492M. Analysis of transcriptomic data and measurements of nutrient uptake/secretion rates were used to generate a GEM descriptive of D492 metabolism pre- and post EMT. The GEMs represent the integrated analysis of 1304 genes and 43 extracellular metabolites and afford a snapshot of D492 metabolism. GEM-based metabolic phenotypes were validated and then used to identify reactions, genes and associated transcription factors that discriminate between D492 epithelial and mesenchymal metabolism. Finally, we used the GEMs to identify genes that when knocked down discriminate between epithelial vs. mesenchymal cell growth. These represent hypotheses of biomarkers or drug targets that could be pursued for anti-metastatic therapy.

Measured uptake rates of metabolites from media were on average higher in D492 and different nutrient distribution profiles within the metabolic networks were observed (Figs. 2 and 5). In particular, altered utilization of carbons originating from glucose, glutamine, arginine and the branched chain amino acids was apparent in the two cell lines on account of altered gene expression in glycolysis and the TCA cycle. Calculation of the most likely carbon flux through metabolic pathways thus indicates that D492 cells rely more on aerobic glycolysis and that activity of anaplerotic reactions associated with the TCA cycle is altered in D492M cells. Measurements of energy metabolites and the measured respiration capacity were consistent with the computed alterations in glycolysis, TCA cycle and pentose phosphate pathway activity. A comparison of reaction flux in the EPI and MES models through reactions corresponding to the mesenchymal metabolic signature (MMS) gene set

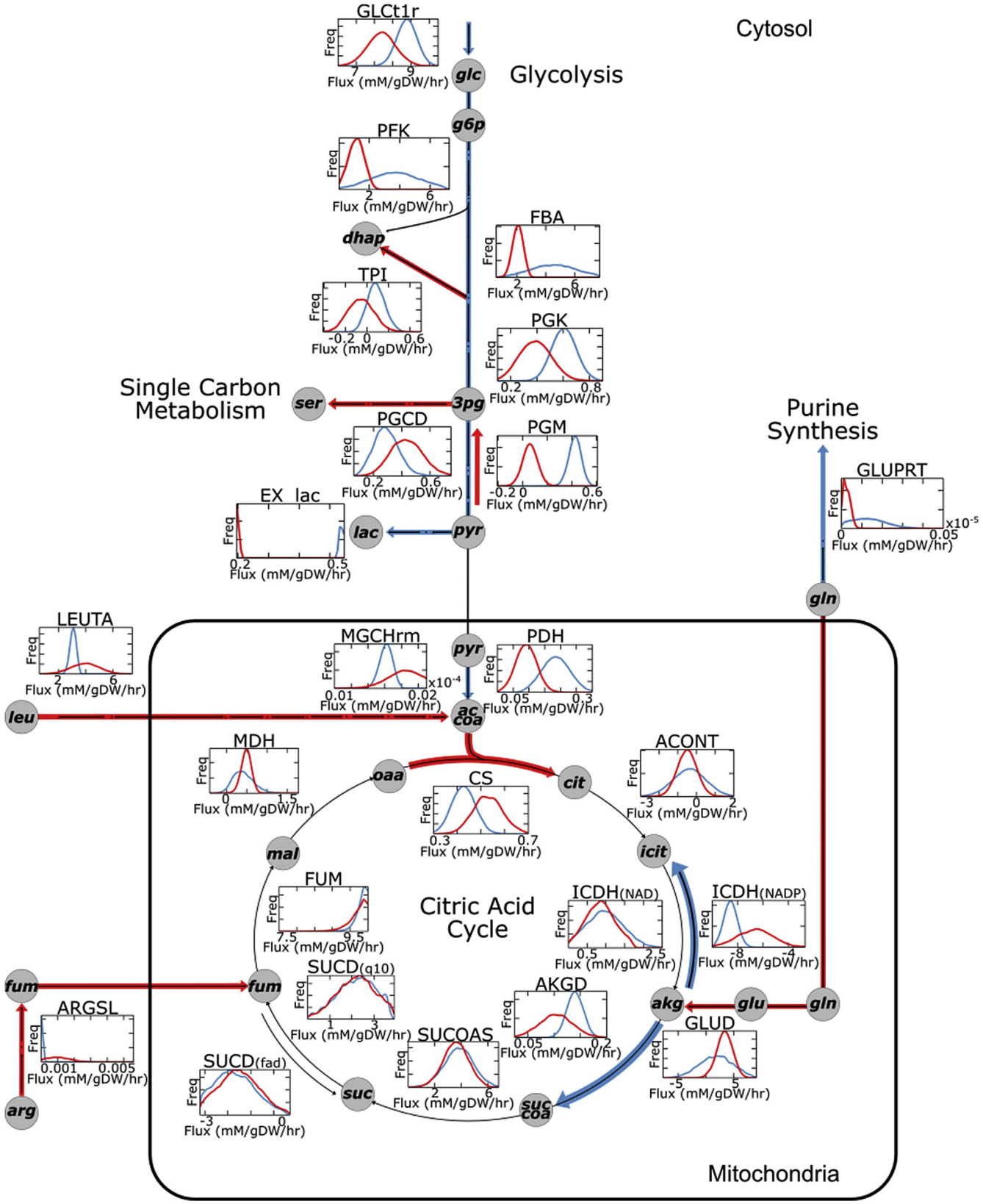

Fig. 5. Predicted flux differences in D492 epithelial and D492M mesenchymal cells. Reactions highlighted in blue carry higher flux in the EPI model while those highlighted in red carry higher flux in the MES model. Reactions in black are identical between the EPI and MES models. Glycolytic flux is higher in the EPI model while carbons are diverted to one carbon metabolism through serine in the MES model. Anaplerotic reaction flux from isoleucine, arginine and glutamine into the TCA cycle is also higher in the MES model. Abbreviations: glc: glucose; g6p: glucose-6-phosphate; dhap: dihydroxyacetone phosphate; 3pg: 3-phosphoglycerate; ser: serine; pyr: pyruvate; lac: lactate; accoa: acetyl-CoA; cit: citrate; akg: alpha-ketoglutarate; suc: succinate; mal: malate; oaa: oxaloacetate; leu: leucine; gln: glutamine; GLCt1r: Glucose transport; FBA: fructose-bisphosphate aldolase; TPI: triose-phosphate isomerase; PGK: phosphoglycerate kinase; PGM: phosphoglycerate mutase; EX_lac: exchange lactate; PGCD: phosphoglycerate dehydrogenase; CS: citrate

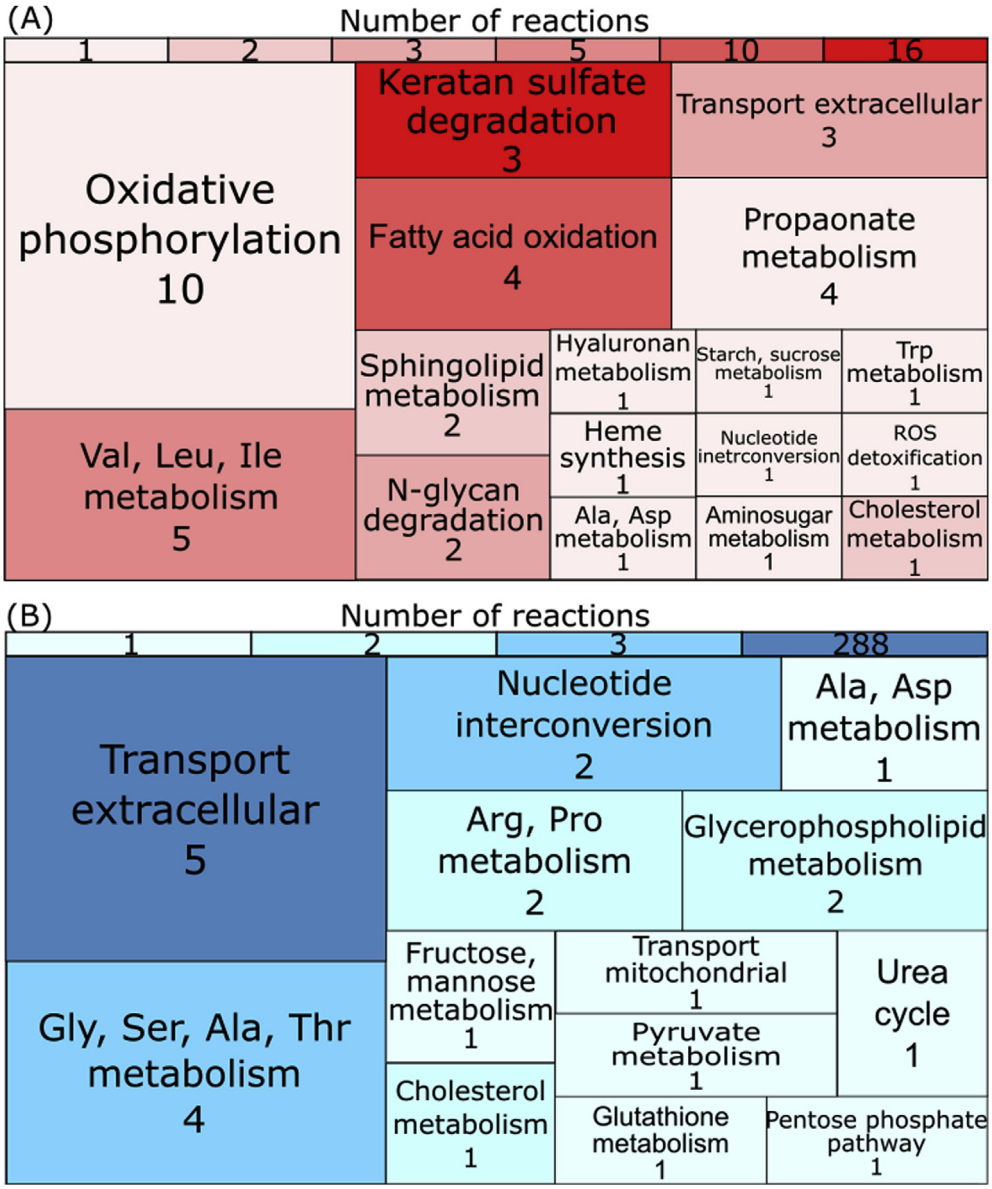

Fig. 6. Tree maps for reaction subsystems involved in EMT (A) and MET (B): The color scale above represents the number of reactions in each subsystem while the size and numbers in the boxes represent the number of genes affecting these reactions.

identified by Shaul et al. [9], showed that out of 19 reactions encoded by the 28 MMS genes present in the two GEMs, 11 had higher flux in the MES model (SI Fig. 6). D492 mesenchymal metabolism thus adheres to the general mesenchymal phenotype although deviations are observed. These deviations are to be expected due to the lack of measurements of metabolites in specific metabolic pathways that contain the MMS encoding reactions and the fact that MMS genes were identified based solely on expression data.

Flux balance analysis of the EPI and MES models suggested that lower proliferation rates of D492M vs. D492 is due to lower cardiolipin synthase activity in the MES model. Cardiolipin is a lipid exclusively found in the inner mitochondrial membrane and is important for mitochondrial function with regard to the formation and maintenance of cristae and formation and stabilization of protein complexes comprising the electron transport chain [26,27]. Although wary of this being a modeling artifact as cardiolipin is part of the biomass function used to optimize model flux, this finding focused our investigation on core energy metabolism. Differences in D492 cell size, weight, mitochondrial staining and respiratory capacity confirmed altered mitochondrial activity (that may or may not arise from altered cardiolipin content), as opposed to a purely quantitative effect induced by fewer mitochondria in D492M. The models therefore correctly

synthase; ACONT: aconitase; ICDH(NAD): isocitrate dehydrogenase (NAD dependent); ICDH(NADP): isocitrate dehydrogenase (NADP dependent); AKGD: alphaketoglutarate dehydrogenase; SUCOAS: succinyl-CoA synthetase; SUCD(fad): succinate dehydrogenase (FAD dependent); SUCD(q10): succinate dehydrogenase (ubiquinone dependent); FUM: fumarase; MDH: malate dehydrogenase; LEUTA: leucine transaminase; MGHCrm: methylglutaconyl-CoA hydratase; GLUPRT: glutamine phosphoribosyldiphosphate amidotransferase; GLUN: glutaminase; ARGSL: argininosuccinate lyase. (For interpretation of the references to color in this figure legend, the reader is referred to the web version of this article.)

Table 2
Genes essential for EPI and MES model: The 13 and 4 genes listed in the table are exclusively essential for the biomass production of EPI model and MES model, respectively.

Essential genes for EPI model growth	
ATP5B	ATP synthase, H+ transporting, mitochondrial F1 complex, beta polypeptide
ATP5I	ATP synthase, H+ transporting, mitochondrial Fo complex subunit E
FH	fumarate hydratase
GCDH	glutaryl-CoA dehydrogenase
GSS	glutathione synthetase
HEXA	hexosaminidase subunit alpha
NSF	N-ethylmaleimide sensitive factor
SDHA	succinate dehydrogenase complex flavoprotein subunit A
SDHB	succinate dehydrogenase complex iron sulfur subunit B
SDHC	succinate dehydrogenase complex subunit C
SDHD	succinate dehydrogenase complex subunit D, integral membrane protein
ATP5L	ATP synthase, H+ transporting, mitochondrial Fo complex subunit G
SLC16A10	solute carrier family 16 member 10
Essential genes for MES model growth	
PDHX	pyruvate dehydrogenase complex component X
ASL	argininosuccinate lyase
SLC7A5	solute carrier family 7 member 5
OAT	ornithine aminotransferase

account for differences in proliferation due to altered mitochondrial activity.

Sampling analysis of the flux space of the D492 GEMs highlighted changes in metabolic pathways (Fig. 6) that have previously been attributed to increased invasiveness of cancer stem cells and EMT including fatty acid oxidation [28], nucleotide interconversions [9] and glycan metabolism [9]. Fatty acid oxidation in particular has been shown to be altered upon loss of attachment of the cells during EMT [28]. Fatty acids are however not equivalent in their impact on cell proliferation [29,30] and more detailed lipid analysis of D492 is required as the D492 models lack intracellular flux measurements of fatty acid oxidation. Regardless, analysis of gene expression data in the context of the models indicate that D492M cells rely considerably more on fatty acid oxidation than D492. Malonyl-CoA decarboxylase is important for breast cancer invasiveness [31] and lipidomic analysis of EMT show vast reorganization of the lipidome consistent with altered membrane fluidity and function following EMT [32]. Expanding the understanding of changes in the lipidome during and following EMT are thus important.

We used the models to identify reactions of importance for EMT and MET in D492 and D492M cells. For this purpose, reactions who's flux requires regulation in order to switch between the EPI and MES model phenotypes were proposed (Fig. 6). Inspection of these reactions and the tracing of calculated metabolite flux values affords mechanistic insight into altered metabolism into the D492 EMT model. For example, the altered activity of TCA anaplerosis predicted by the models was traced to amino acid metabolism arising from differential uptake rates of arginine, threonine, lysine and leucine and/or isoleucine. Leucine/isoleucine and arginine induce the activation of mTOR that is associated with enhanced proliferation which we did not observe in D492M. In light of the lower ATP concentration in D492M and lower proliferation rate we conclude that increased uptake of leucine/isoleucine (and arginine) in D492M reflects altered metabolism in D492 associated with differentiation rather than proliferation. Indeed, the models predict that these metabolites are metabolized differently within the two cell lines. According to the model predictions, arginine was used to generate fumarate and proline through citruline and ornithine respectively. In the EPI model however, arginine fuels polyamine synthesis through ornithine, consistent with enhanced polyamine requirement for proliferation [33]. Lysine is oxidized in both models to acetyl CoA in the mitochondria through 2-oxoadipate, however only in the MES model was lysine utilized to generate allysine, a component of elastin and collagen. Threonine was oxidized through propanoyl-CoA in both models, but again appears to be more important in the fueling of the TCA cycle in the MES model.

We also identified enzymatic reactions of interest outside central carbon metabolism that have previously been associated with EMT. Specifically, for glycan and keratan sulfate degradation we identified FucA1. FucA1 is de-regulated in TGF-β induced EMT in bladder epithelial cells [34] and fucosylation of E-cadherin has been shown to impact cell migration in lung cancer cells [35] and is a biomarker for cellular senescence [36]. The proposed increased flux through glycan degradation pathways in D492M is consistent with these results. Similarly, delta (14)sterol reductase, a key enzyme in cholesterol synthesis, encoded by TM7SF2, previously identified as a signature mesenchymal marker [9], was identified as important for EMT reflecting the increased requirement for membrane fluidity in mesenchymal cells. Prolonged statin therapy has previously been shown to increase breast cancer incidence [37]. However, our results support epidemiologic evidence of the protective effect of statins on breast cancer recurrence [38], presumably through inhibition of EMT. These findings require follow up molecular biology based investigation. Interestingly, TM7SF2 was recently found to correlate with NFKB and TNF-α expression in mouse fibroblasts [39]. TNF-α induces EMT through upregulation of TWIST via NFKB.

Reports on alterations in core energy metabolism in cells undergoing EMT are conflicting and have been associated with both increased and decreased anaerobic glycolysis and increased and decreased proliferation [40,41]. Specifically, our results do not agree with similar investigations of EMT using the HER2 positive BT-474 and ER positive MCF7 EMT cell culture models that found increased proliferation and a switch to aerobic glycolysis following EMT [42]. This highlights the metabolic diversity of EMT cell models that we have recently shown is influenced by heterogeneous expression profiles in EGFR signaling and is consistent with the inherent flexibility and variation characteristic of EMT [43]. The D492/D492M model of EMT presents an alternative to commonly used cell models of EMT such as HMLE, BT-474 and MCF7 [44] [42,45]. This is important given the heterogeneity of cell models used in EMT studies [13] and may contribute to the understanding the metabolic diversity of EMT. Altered metabolism may also relate to the breast cancer sub-type under study. D492 is representative of basal like breast cancer that has similarities to triple negative breast cancer [46]. Ultimately, because the D492 cell model allows investigation of epithelial cells pre- and post EMT, our results suggest that in the context of D492, enhanced glycolysis is not a required for maintaining the mesenchymal phenotype.

Importantly, neither D492 nor D492M cells are tumorigenic. D492 originates from reduction mammoplasty, immortalized with E6/E7 viral transduction [47]. D492M has a distinct mesenchymal-like phenotype and does not revert back to the original epithelial phenotype. It should be kept in mind that although tumor development is associated with increased cell proliferation and growth, the change to an invasive, mesenchymal phenotype is not [48]. While EMT is believed to be a pre-requisite to tumor invasion and metastasis, the reversion of mesenchymal cells back to epithelial (MET) is thought to be a crucial step in the formation of secondary tumors [49]. Another equally important role of EMT in cancer progression may be its contribution to chemoresistance. A recent publication by Fischer et al. elegantly demonstrated that EMT is in fact not a prerequisite for secondary tumor formation in a mouse breast cancer model [50]. However, treatment with cyclophosphamide produced a population of EMT derived mesenchymal cells

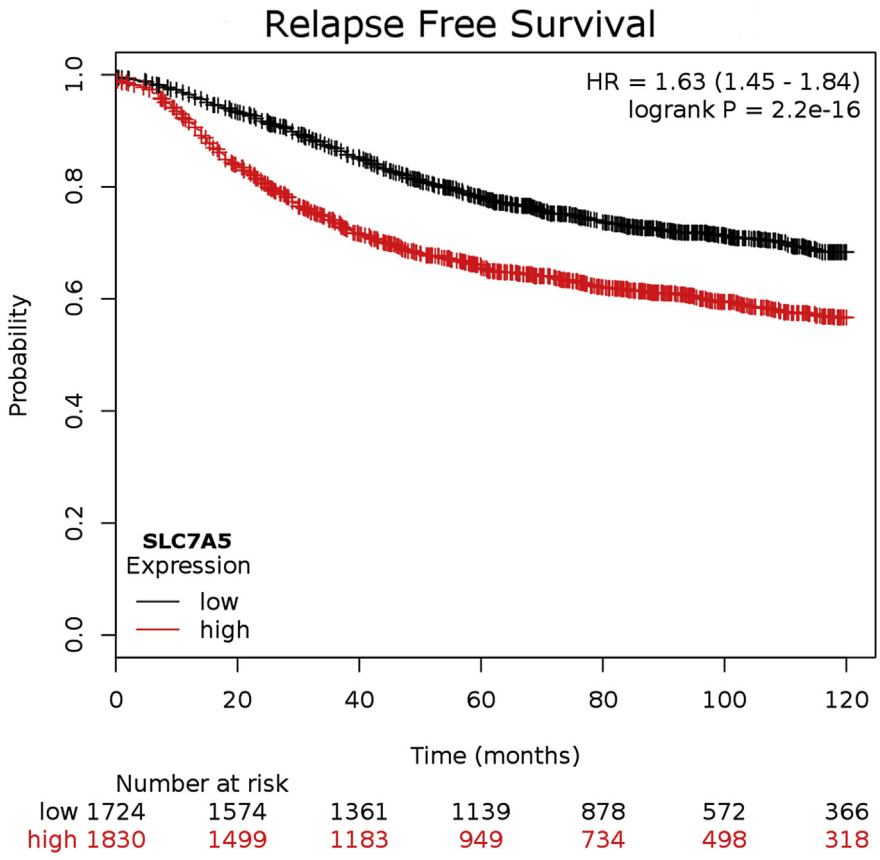

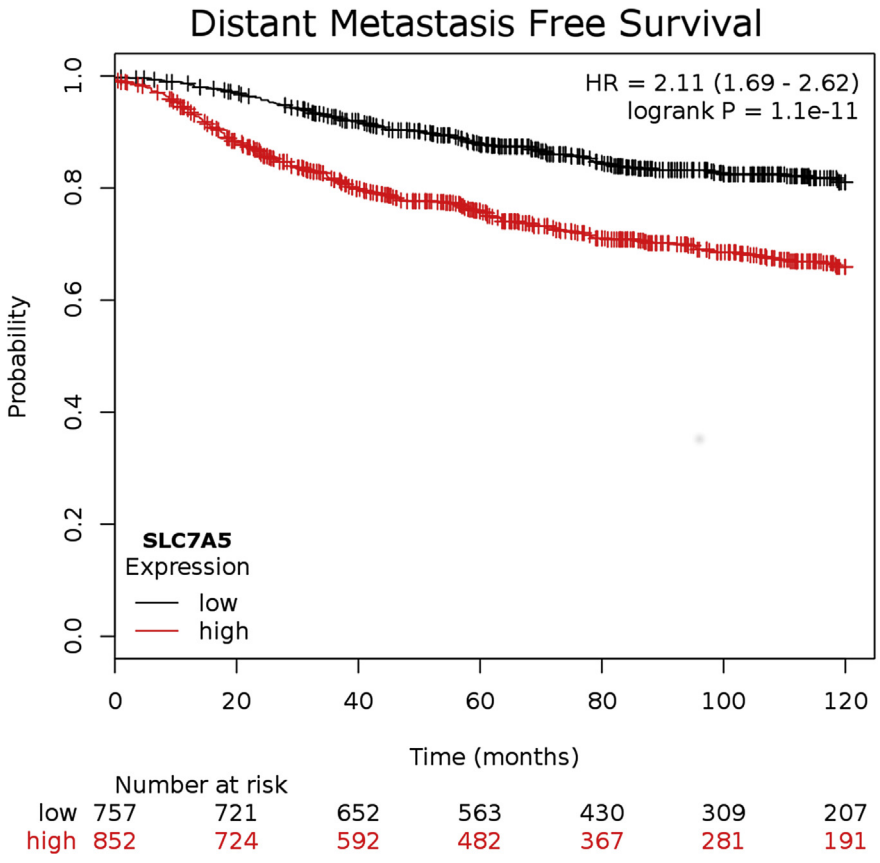

Fig. 7. High expression of the SLC7A5 subunit of the LAT1 transport system negatively correlates with breast cancer prognosis. Kaplan–Meier survival curves for relapse free and distant metastasis free survival based on high or low SLC7A5 expression. 3554 tumors were evaluated for SLC7A5 expression and correlated with risk of relapse (left), 1609 tumors were evaluated for SLC7A5 expression and risk of developing cancers elsewhere in the body. In both cases, high expression of SLC7A5 predicts worse prognosis.

that were resistant to treatment and could potentially initiate new tumors after treatment. The D492/D492M cell model is therefore an ideal system to explore the metabolic re-wiring that takes place during EMT and should not be viewed as a tool to examine secondary tumor growth.

SLC7A5 was identified as one of the 4 genes essential for growth of the MES model but not essential for the EPI model (Table 2). SLC7A5 is one of two subunits of LAT1, a high affinity transport system for large neutral amino. Inhibition of SLC7A5 would therefore be predicted to specifically inhibit the growth of D492M cells and in effect, inhibit EMT in this cell system. The LAT1 transport system has been implicated as a negative prognostic marker in a number of cancers including prostate adenocarcinoma [51], biliary tract cancer [52], multiple myeloma [53], hypopharyngeal squamous cell carcinoma [54], adenoid cystic carcinoma [55], metastatic lung cancer [56] and triple negative breast cancer [57]. Inhibition or knockdown of LAT1 in KKU-M213 biliary tract carcinoma cells has been shown to reduce migration and invasion *in vitro* [58]. We show that higher SLC7A5 expression correlated with increased risk of cancer relapse and distant metastasis formation (Fig. 7) in a cohort of 3557 breast cancer patients. We believe that the results presented here and by others warrant further investigation into the potential therapeutic use of SLC7A5 or LAT1 inhibitors as inhibitors of cancer growth or metastasis.

The curated GEMs of D492 are the first that are representative of metabolism of EMT generated to date and serve to characterize the metabolism of the D492 EMT cell model. Although the generation of metabolic models is now commonplace using automated algorithms [59], the model generated here was manually curated and the computed metabolic phenotypes were experimentally validated. These GEMs therefore represent a foundation for future constraint based analysis of epithelial and mesenchymal metabolism within or outside the context of EMT. Furthermore, the methodology used to generate the two models is novel and presents an alternative approach to building context-specific GEMs. As opposed to directly constraining a generic reaction knowledgebase such as RECON2 or the human metabolic atlas [60], we used a combined transcriptomic dataset descriptive of metabolic reaction content in both cell lines as a basis for model construction (the EMT model) that we then further constrained to generate the GEMs descriptive of D492 and D492M metabolism (the EPI and MES models). The approach allows direct comparison of metabolic phenotypes upon a curated context specific reconstruction that is of value when modeling biological events such as EMT where alternative expression off the same genetic background is being investigated, for example during embryonic development and stem cell differentiation.

Although our experimental setup was conducted in monolayer, we acknowledge that tissue-context can be of great importance. By performing studies such as this one in three dimensional reconstituted basement membrane (3DrBM) matrix, it is possible to recapture the phenotypic form of *in vivo*-like structures. In that regard it has previously been shown that gene expression varies significantly between monolayer and 3D culture [61] and glucose metabolism is altered between 2D and 3D culture [62]. Experimental conditions in general are of importance when designing studies that combine multiple large datasets. All experiments used for data generation should be conducted in the same manner; gene expression profiling, enzymatic assays and metabolomics profiling must capture the same state of cell culture [63]. Ideally, cell culture medium should replicate *in vivo* conditions, providing cells with all the necessary components to maintain and replicate without providing excessive amounts of nutrients and/or growth factors. However, cell culture often relies on mediums containing nutrients and growth factors in excess that favor rapid, continuous growth of cells, rather than biological representation. This in turn may lead to biochemical activities within the cells that are not representative of *in vivo* events [64]. Previous efforts have been made to tailor medium composition to the specific needs of the cells in question based in metabolic profiling, resulting in a culture medium that was more biologically relevant and allowed increased sensitivity in drug screening assays [64]. Studies such as this one, although performed in rich medium, set a baseline for nutritional needs of breast epithelial cell lines and may facilitate future development of more biologically relevant culture medium.

Funding

Financial support for this work was provided by the Icelandic Research Council (Grants number: 130591-051, 130816-051 and 152358-051).

Conflict of interest

Authors state that there are no conflicts of interest to disclose.

Acknowledgments

We thank Dr. Giuseppe Paglia for valuable discussions on metabolomics experimental design and Dr. Guðmundur Logi Norddahl for help with flow cytometry.

Appendix A. Supplementary data

Supplementary data related to this article can be found at http://dx.doi.org/10.1016/j.canlet.2017.03.019.

References

[1] R. Kalluri, EMT: when epithelial cells decide to become mesenchymal-like cells, J. Clin. Invest. 119 (2009) 1417–1419.
[2] R. Kalluri, R.A. Weinberg, The basics of epithelial-mesenchymal transition, J. Clin. Invest. 119 (2009) 1420–1428.
[3] H. Acloque, M.S. Adams, K. Fishwick, M. Bronner-Fraser, M.A. Nieto, Epithelial-mesenchymal transitions: the importance of changing cell state in development and disease, J. Clin. Invest. 119 (2009) 1438–1449.
[4] K. Polyak, R.A. Weinberg, Transitions between epithelial and mesenchymal states: acquisition of malignant and stem cell traits, Nat. Rev. Cancer 9 (2009) 265–273.
[5] O.W. Petersen, H.L. Nielsen, T. Gudjonsson, R. Villadsen, F. Rank, E. Niebuhr, et al., Epithelial to mesenchymal transition in human breast cancer can provide a nonmalignant stroma, Am. J. Pathol. 162 (2003) 391–402.
[6] G. Barriere, P. Fici, G. Gallerani, F. Fabbri, M. Rigaud, Epithelial mesenchymal transition: a double-edged sword, Clin. Transl. Med. 4 (2015) 14.
[7] C. Dong, T. Yuan, Y. Wu, Y. Wang, T.W. Fan, S. Miriyala, et al., Loss of FBP1 by Snail-mediated repression provides metabolic advantages in basal-like breast cancer, Cancer Cell 23 (2013) 316–331.
[8] J. Hanai, N. Doro, A.T. Sasaki, S. Kobayashi, L.C. Cantley, P. Seth, et al., Inhibition of lung cancer growth: ATP citrate lyase knockdown and statin treatment leads to dual blockade of mitogen-activated protein kinase (MAPK) and phosphatidylinositol-3-kinase (PI3K)/AKT pathways, J. Cell. Physiol. 227 (2012) 1709–1720.
[9] Y.D. Shaul, E. Freinkman, W.C. Comb, J.R. Cantor, W.L. Tam, P. Thiru, et al., Dihydropyrimidine accumulation is required for the epithelial-mesenchymal transition, Cell 158 (2014) 1094–1109.
[10] E.J. O'Brien, J.M. Monk, B.O. Palsson, Using genome-scale models to predict biological capabilities, Cell 161 (2015) 971–987.
[11] B.O. Palsson, Systems Biology: Constraint-based Reconstruction and Analysis, Cambridge University Press, 2015.
[12] K. Yizhak, S.E. Le Devedec, V.M. Rogkoti, F. Baenke, V.C. de Boer, C. Frezza, et al., A computational study of the Warburg effect identifies metabolic targets inhibiting cancer migration, Mol. Syst. Biol. 10 (2014) 744.
[13] K.S. Choudhary, N. Rohatgi, S. Halldorsson, E. Briem, T. Gudjonsson, S. Gudmundsson, et al., EGFR signal-network reconstruction demonstrates metabolic crosstalk in EMT, PLoS Comput. Biol. 12 (2016) e1004924.
[14] V. Sigurdsson, B. Hilmarsdottir, H. Sigmundsdottir, A.J. Fridriksdottir, M. Ringner, R. Villadsen, et al., Endothelial induced EMT in breast epithelial cells with stem cell properties, PLoS One 6 (2011) e23833.

[15] G. Paglia, O.E. Sigurjonsson, O. Rolfsson, S. Valgeirsdottir, M.B. Hansen, S. Brynjolfsson, et al., Comprehensive metabolomic study of platelets reveals the expression of discrete metabolic phenotypes during storage, Transfusion 54 (2014) 2911–2923.
[16] M. Jain, R. Nilsson, S. Sharma, N. Madhusudhan, T. Kitami, A.L. Souza, et al., Metabolite profiling identifies a key role for glycine in rapid cancer cell proliferation, Science 336 (2012) 1040–1044.
[17] I. Thiele, N. Swainston, R.M. Fleming, A. Hoppe, S. Sahoo, M.K. Aurich, et al., A community-driven global reconstruction of human metabolism, Nat. Biotechnol. 31 (2013) 419–425.
[18] N. Vlassis, M.P. Pacheco, T. Sauter, Fast reconstruction of compact context-specific metabolic network models, PLoS Comput. Biol. 10 (2014) e1003424.
[19] D.A. Fell, J.R. Small, Fat synthesis in adipose tissue. An examination of stoichiometric constraints, Biochem. J. 238 (1986) 781–786.
[20] J.M. Savinell, B.O. Palsson, Network analysis of intermediary metabolism using linear optimization. I. Development of mathematical formalism, J. Theor. Biol. 154 (1992) 421–454.
[21] J. Schellenberger, B.O. Palsson, Use of randomized sampling for analysis of metabolic networks, J. Biol. Chem. 284 (2009) 5457–5461.
[22] D. Lee, K. Smallbone, W.B. Dunn, E. Murabito, C.L. Winder, D.B. Kell, et al., Improving metabolic flux predictions using absolute gene expression data, BMC Syst. Biol. 6 (2012).
[23] J. Fuxe, T. Vincent, A. Garcia de Herreros, Transcriptional crosstalk between TGF-beta and stem cell pathways in tumor cell invasion: role of EMT promoting Smad complexes, Cell Cycle 9 (2010) 2363–2374.
[24] N. Kolesnikoff, J.L. Attema, S. Roslan, A.G. Bert, Q.P. Schwarz, P.A. Gregory, et al., Specificity protein 1 (Sp1) maintains basal epithelial expression of the miR-200 family: implications for epithelial-mesenchymal transition, J. Biol. Chem. 289 (2014) 11194–11205.
[25] B. Gyorffy, A. Lanczky, A.C. Eklund, C. Denkert, J. Budczies, Q. Li, et al., An online survival analysis tool to rapidly assess the effect of 22,277 genes on breast cancer prognosis using microarray data of 1,809 patients, Breast Cancer Res. Treat. 123 (2010) 725–731.
[26] E.M. Mejia, G.M. Hatch, Mitochondrial phospholipids: role in mitochondrial function, J. Bioenerg. Biomembr. 48 (2016) 99–112.
[27] G. Paradies, V. Paradies, V. De Benedictis, F.M. Ruggiero, G. Petrosillo, Functional role of cardiolipin in mitochondrial bioenergetics, Biochim. Biophys. Acta 1837 (2014) 408–417.
[28] C.L. Buchheit, K.J. Weigel, Z.T. Schafer, OPINION Cancer cell survival during detachment from the ECM: multiple barriers to tumour progression, Nat. Rev. Cancer 14 (2014) 632–641.
[29] S. Hardy, W. El-Assaad, E. Przybytkowski, E. Joly, M. Prentki, Y. Langelier, Saturated fatty acid-induced apoptosis in MDA-MB-231 breast cancer cells. A role for cardiolipin, J. Biol. Chem. 278 (2003) 31861–31870.
[30] Z.T. Schug, B. Peck, D.T. Jones, Q. Zhang, S. Grosskurth, I.S. Alam, et al., Acetyl-CoA synthetase 2 promotes acetate utilization and maintains cancer cell growth under metabolic stress, Cancer Cell 27 (2015) 57–71.
[31] K. Yizhak, E. Gaude, S. Le Devedec, Y.Y. Waldman, G.Y. Stein, B. van de Water, et al., Phenotype-based cell-specific metabolic modeling reveals metabolic liabilities of cancer, eLife 3 (2014).
[32] W. Zhao, S. Prijic, B.C. Urban, M.J. Tisza, Y. Zuo, L. Li, et al., Candidate antimetastasis drugs suppress the metastatic capacity of breast cancer cells by reducing membrane fluidity, Cancer Res. 76 (2016) 2037–2049.
[33] K. Soda, The mechanisms by which polyamines accelerate tumor spread, J. Exp. Clin. Cancer Res. 30 (2011) 95.
[34] J. Guo, X. Li, Z. Tan, W. Lu, G. Yang, F. Guan, Alteration of N-glycans and expression of their related glycogenes in the epithelial-mesenchymal transition of HCV29 bladder epithelial cells, Molecules 19 (2014) 20073–20090.
[35] K. Shao, Z.Y. Chen, S. Gautam, N.H. Deng, Y. Zhou, X.Z. Wu, Posttranslational modification of E-cadherin by core fucosylation regulates Src activation and induces epithelial-mesenchymal transition-like process in lung cancer cells, Glycobiology 26 (2016) 142–154.
[36] D. Hildebrand, S. Lehle, A. Borst, S. Haferkamp, F. Essmann, K. Schulze-Osthoff, α-Fucosidase as a novel convenient biomarker for cellular senescence, Cell Cycle 12 (2013) 1922–1927.
[37] J.A. McDougall, K.E. Malone, J.R. Daling, K.L. Cushing-Haugen, P.L. Porter, C.I. Li, Long-term statin use and risk of ductal and lobular breast cancer among women 55 to 74 years of age, Cancer Epidemiol. Biomarkers Prev. 22 (2013) 1529–1537.
[38] T.P. Ahern, T.L. Lash, P. Damkier, P.M. Christiansen, D.P. Cronin-Fenton, Statins and breast cancer prognosis: evidence and opportunities, Lancet Oncol. 15 (2014) e461–e468.
[39] I. Bellezza, R. Roberti, L. Gatticchi, R. Del Sordo, M.G. Rambotti, M.C. Marchetti, et al., A novel role for Tm7sf2 gene in regulating TNFalpha expression, PLoS One 8 (2013) e68017.
[40] S. Thomson, F. Petti, I. Sujka-Kwok, P. Mercado, J. Bean, M. Monaghan, et al., A systems view of epithelial-mesenchymal transition signaling states, Clin. Exp. Metastasis 28 (2011) 137–155.
[41] L. Jerby, L. Wolf, C. Denkert, G.Y. Stein, M. Hilvo, M. Oresic, et al., Metabolic associations of reduced proliferation and oxidative stress in advanced breast cancer, Cancer Res. 72 (2012) 5712–5720.
[42] Y. Kondaveeti, I.K. Guttilla Reed, B.A. White, Epithelial-mesenchymal transition induces similar metabolic alterations in two independent breast cancer cell lines, Cancer Lett. 364 (2015) 44–58.
[43] S. Lamouille, J. Xu, R. Derynck, Molecular mechanisms of epithelial-mesenchymal transition, Nat. Rev. Mol. Cell Biol. 15 (2014) 178–196.
[44] S.A. Mani, W. Guo, M.J. Liao, E.N. Eaton, A. Ayyanan, A.Y. Zhou, et al., The epithelial-mesenchymal transition generates cells with properties of stem cells, Cell 133 (2008) 704–715.
[45] W.L. Tam, H. Lu, J. Buikhuisen, B.S. Soh, E. Lim, F. Reinhardt, et al., Protein kinase C alpha is a central signaling node and therapeutic target for breast cancer stem cells, Cancer Cell 24 (2013) 347–364.
[46] S. Badve, D.J. Dabbs, S.J. Schnitt, F.L. Baehner, T. Decker, V. Eusebi, et al., Basal-like and triple-negative breast cancers: a critical review with an emphasis on the implications for pathologists and oncologists, Mod. Pathol. 24 (2011) 157–167.
[47] T. Gudjonsson, R. Villadsen, H.L. Nielsen, L. Ronnov-Jessen, M.J. Bissell, O.W. Petersen, Isolation, immortalization, and characterization of a human breast epithelial cell line with stem cell properties, Genes Dev. 16 (2002) 693–706.
[48] T. Funasaka, H. Hu, T. Yanagawa, V. Hogan, A. Raz, Down-regulation of phosphoglucose isomerase/autocrine motility factor results in mesenchymal-to-epithelial transition of human lung fibrosarcoma cells, Cancer Res. 67 (2007) 4236–4243.
[49] M. Luo, M. Brooks, M.S. Wicha, Epithelial-mesenchymal plasticity of breast cancer stem cells: implications for metastasis and therapeutic resistance, Curr. Pharm. Des. 21 (2015) 1301–1310.
[50] K.R. Fischer, A. Durrans, S. Lee, J. Sheng, F. Li, S.T. Wong, et al., Epithelial-to-mesenchymal transition is not required for lung metastasis but contributes to chemoresistance, Nature 527 (2015) 472–476.
[51] N. Yanagisawa, T. Satoh, K. Hana, M. Ichinoe, N. Nakada, H. Endou, et al., L-amino acid transporter 1 may be a prognostic marker for local progression of prostatic cancer under expectant management, Cancer Biomark. 15 (2015) 365–374.
[52] K. Kaira, Y. Sunose, N. Oriuchi, Y. Kanai, I. Takeyoshi, CD98 is a promising prognostic biomarker in biliary tract cancer, Hepatobiliary Pancreat. Dis. Int. 13 (2014) 654–657.
[53] A. Isoda, K. Kaira, M. Iwashina, N. Oriuchi, H. Tominaga, S. Nagamori, et al., Expression of L-type amino acid transporter 1 (LAT1) as a prognostic and therapeutic indicator in multiple myeloma, Cancer Sci. 105 (2014) 1496–1502.
[54] M. Toyoda, K. Kaira, M. Shino, K. Sakakura, K. Takahashi, Y. Takayasu, et al., CD98 as a novel prognostic indicator for patients with stage III/IV hypopharyngeal squamous cell carcinoma, Head Neck 37 (2015) 1569–1574.
[55] K. Kaira, M. Toyoda, M. Shino, K. Sakakura, K. Takahashi, H. Tominaga, et al., Clinicopathological significance of L-type amino acid transporter 1 (LAT1) expression in patients with adenoid cystic carcinoma, Pathol. Oncol. Res. 19 (2013) 649–656.
[56] K. Kaira, N. Oriuchi, H. Imai, K. Shimizu, N. Yanagitani, N. Sunaga, et al., CD98 expression is associated with poor prognosis in resected non-small-cell lung cancer with lymph node metastases, Ann. Surg. Oncol. 16 (2009) 3473–3481.
[57] M. Furuya, J. Horiguchi, H. Nakajima, Y. Kanai, T. Oyama, Correlation of L-type amino acid transporter 1 and CD98 expression with triple negative breast cancer prognosis, Cancer Sci. 103 (2012) 382–389.
[58] K. Janpipatkul, K. Suksen, S. Borwornpinyo, N. Jearawiriyapaisarn, S. Hongeng, P. Piyachaturawat, et al., Downregulation of LAT1 expression suppresses cholangiocarcinoma cell invasion and migration, Cell. Signal. 26 (2014) 1668–1679.
[59] L. Jerby, E. Ruppin, Predicting drug targets and biomarkers of cancer via genome-scale metabolic modeling, Clin. Cancer Res. 18 (2012) 5572–5584.
[60] D. Machado, M. Herrgard, Systematic evaluation of methods for integration of transcriptomic data into constraint-based models of metabolism, Plos Comput. Biol. 10 (2014).
[61] M. Yu, G. Lin, N. Arshadi, I. Kalatskaya, B. Xue, S. Haider, et al., Expression profiling during mammary epithelial cell three-dimensional morphogenesis identifies PTPRO as a novel regulator of morphogenesis and ErbB2-mediated transformation, Mol. Cell. Biol. 32 (2012) 3913–3924.
[62] Y. Onodera, J.M. Nam, M.J. Bissell, Increased sugar uptake promotes oncogenesis via EPAC/RAP1 and O-GlcNAc pathways, J. Clin. Invest. 124 (2014) 367–384.
[63] Z. Leon, J.C. Garcia-Canaveras, M.T. Donato, A. Lahoz, Mammalian cell metabolomics: experimental design and sample preparation, Electrophoresis 34 (2013) 2762–2775.
[64] D.J. Creek, B. Nijagal, D.H. Kim, F. Rojas, K.R. Matthews, M.P. Barrett, Metabolomics guides rational development of a simplified cell culture medium for drug screening against Trypanosoma brucei, Antimicrob. Agents Chemother. 57 (2013) 2768–2779.